NASA/CR-1998-208964
ICASE Report No. 98-56

Rayleigh-Bénard Simulation using Gas-kinetic BGK Scheme in the Incompressible Limit

Kun Xu
ICASE, Hampton, Virginia
and
The Hong Kong University of Science and Technology, Hong Kong

Shiu-Hong Lui
The Hong Kong University of Science and Technology, Hong Kong

Institute for Computer Applications in Science and Engineering
NASA Langley Research Center
Hampton, VA

Operated by Universities Space Research Association

National Aeronautics and
Space Administration

Langley Research Center
Hampton, Virginia 23681-2199

Prepared for Langley Research Center
under Contract NAS1-97046

December 1998

RAYLEIGH-BÉNARD SIMULATION USING GAS-KINETIC BGK SCHEME IN THE INCOMPRESSIBLE LIMIT *

KUN XU† AND SHIU-HONG LUI‡

Abstract. In this paper, a gas-kinetic BGK model is constructed for the Rayleigh-Bénard thermal convection in the incompressible flow limit, where the flow field and temperature field are described by two coupled BGK models. Since the collision times and pseudo-temperature in the corresponding BGK models can be different, the Prandtl number can be changed to any value instead of a fixed Pr = 1 in the original BGK model. The 2D Rayleigh-Bénard thermal convection is studied and numerical results are compared with theoretical ones as well as other simulation results.

Key words. thermal instability, incompressible flow, gas-kinetic scheme

Subject classification. Applied Numerical Mathematics

1. Introduction. The use of a code for compressible flow to study incompressible fluid has attracted much attention in the past years. Since compressibility is proportional to the Mach number squared, $\delta\rho/\rho \sim M^2$, it is negligible once the Mach number is lower than 0.15. In many numerical test cases, such as the cavity flow, the results from compressible codes are almost identical to the results from incompressible codes[3, 9, 13]. It is also realized that using a compressible code for incompressible simulations have advantages. For example, a Poisson solver is avoided and parallelization of the code can be easily implemented.

If thermal effects are involved in the incompressible flow, a simple adaptation of a compressible code here bears potential danger. The reason is that the density varies with the temperature; this variation cannot in general be neglected, and therefore, even at small velocities, the density of a non-uniformly heated fluid cannot be supposed constant. For example, across the thermal boundary layer, the pressure is almost constant. If the temperature changes substantially, say by 10%, in the layer, then the energy equation will cause a 10% density change due to the ideal equation of state $p = \rho RT$. In reality, the density change is minimal with any reasonable temperature variation in the liquid. So, the compressibility effect is more severe in the thermal problem than that for the pure Mach compression problem where $\delta\rho/\rho \sim M^2$. It is certainly true that we can use other equations of state to describe a slightly compressible liquid. See [10] and references therein. There, the ability to recover the correct thermal effects is still questionable. In most current literature about the application of compressible codes to incompressible flows, thermal compressibility seems to be ignored.

In order to reduce the compressibility in the compressible code for the thermal problem, we have to, in some ways, decouple the mass and momentum from the energy equation. In this paper, two pseudo-temperatures are used to model the Rayleigh-Bénard thermal convection problem in the incompressible

* This research was supported by the National Aeronautics and Space Administration under NASA Contract No. NAS1-97046 while the author was in residence at the Institute for Computer Applications in Science and Engineering (ICASE), NASA Langley Research Center, Hampton, VA 23681-2199. Additional support was provided by Hong Kong Research Grant Council through RGC97/98.HKUST6166/97P.

†Institute for Computer Applications in Science and Engineering, Mail Stop 403, NASA Langley Research Center, Hampton, VA 23681-2199 (email: kxu@icase.edu), and Mathematics Department, the Hong Kong University of Science and Technology, Kowloon, Hong Kong (email:makxu@uxmail.ust.hk).

‡ Mathematics Department, The Hong Kong University of Science and Technology, Kowloon Hong Kong (email:shlui@uxmail.ust.hk).

limit. In the current model, the velocity field and temperature field are described by two BGK models with different collision times. As a consequence, the Prandtl number can be changed to any value by modifying the collision times.

2. Gas-Kinetic BGK Models for Rayleigh Bénard Thermal Convection. In this section, we are going to construct BGK models to study the following incompressible Navier-Stokes equations with thermal effect,

$$\begin{cases} \frac{\partial \rho}{\partial t} + \nabla \cdot (\rho \mathbf{U}) = 0, \\ \frac{\partial \mathbf{U}}{\partial t} + \mathbf{U} \cdot \nabla \mathbf{U} = -\frac{\nabla p}{\rho} + \nu \nabla^2 \mathbf{U} - \mathbf{G}, \\ \frac{\partial (\rho T)}{\partial t} + \nabla \cdot (\rho T \mathbf{U}) = \nabla \cdot (k \nabla T), \end{cases} \tag{2.1}$$

where ρ is the density which is a constant in the incompressible limit, $\mathbf{U}$ the velocity, p the pressure, k the coefficient of thermal conductivity, and T the temperature. Note that ρT is the thermal energy. For the Rayleigh-Bénard convection in a two-dimensional box, the Boussinesq approximation gives

$$\rho \mathbf{G} = \rho \beta G_0 (T - T_m) \hat{y},$$

where G_0 is the gravitational constant, T_m the average value of the top and bottom temperatures, $\hat{y}$ the unit vector in the vertical direction, and β the coefficient of volume expansion. For authoritative treatments of this problem, see, for example, [2] and [6].

In order to the recover the above equations, gas-kinetic models can be constructed in the following forms,

$$\frac{\partial f}{\partial t} + \mathbf{u} \cdot \nabla f = \frac{f^{eq} - f}{\tau_\nu} + F, \tag{2.2}$$

$$\frac{\partial h}{\partial t} + \mathbf{u} \cdot \nabla h = \frac{h^{eq} - h}{\tau_c}, \tag{2.3}$$

where $\mathbf{u} = (u, v)$ is the x and y components of the particle velocity. Eq.(2.2) is used to recover the mass and momentum equations, and also the velocity flow field. Eq.(2.3) is for the thermal energy evolution. The equilibrium states f^{eq} and h^{eq} have the following forms

$$f^{eq} = \rho (\frac{\lambda_1}{\pi}) e^{-\lambda_1 ((\mathbf{u}-\mathbf{U})^2)},$$

$$h^{eq} = \rho T (\frac{\lambda_2}{\pi}) e^{-\lambda_2 ((\mathbf{u}-\mathbf{U})^2)}$$

where λ_1 and λ_2 can be expressed as

$$\lambda_1 = \frac{1}{2RT_1} \qquad \text{and} \qquad \lambda_2 = \frac{1}{2RT_2},$$

with the two pseudo-temperatures T_1 and T_2. Here T is the real temperature to be simulated. Note that T_1 and T_2 are both constants in the current model, and the value of either T_1 or λ_1 determines the artificial sound speed of the flow field. In the above BGK models, the compressibility is determined from Eq.(2.2) with the equation of state $p = \rho R T_1$, which is totally decoupled from the real temperature T. The external forcing term F in Eq.(2.2) can be approximated as [7],

$$F = 2\lambda \mathbf{G} \cdot (\mathbf{u} - \mathbf{U}) f^{eq},$$

from which the buoyancy force can be recovered.

In the course of particle collisions, the compatibility condition is satisfied in the BGK models,

$$\int (f^{eq} - f) \begin{pmatrix} 1 \\ u \\ v \end{pmatrix} dudv = 0,$$

and

$$\int (h^{eq} - h) dudv = 0.$$

By using Chapman-Enskog expansion, Eq.(2.1) can be recovered exactly in the incompressible limit, with the viscosity coefficient

$$\nu = \tau_\nu \rho R T_1$$

and the heat conduction coefficient

$$k = \tau_c \rho R T_2.$$

Different from the original BGK model[1], here both coefficients are decoupled from the fluid temperature T. As a result, the Prandtl number Pr becomes

$$Pr = \frac{\nu}{k} = \frac{\tau_\nu}{\tau_c} \frac{T_1}{T_2},$$

which can be changed to any value by choosing different τ_ν, τ_c, T_1, or T_2.

3. Numerical Scheme for the BGK Models. For a finite volume scheme, we need to evaluate the numerical fluxes across a cell interface, and the flux function depends on the gas distribution function. In this section, the BGK scheme to solve Eq.(2.2) and (2.3) for fluxes will be presented.

Firstly, for Eq.(2.2) we are going to use the operator splitting method to solve the equation into two steps

$$f_t + u f_x + v f_y = \frac{f^{eq} - f}{\tau_\nu}, \tag{3.1}$$

and

$$f_t = F. \tag{3.2}$$

For Eq.(3.1), in the smooth incompressible limit, the general solution of f in the above equation at the cell interface $x_{i+1/2,j}$ and time t can be simplified as[15],

$$f(x_{i+1/2,j}, y_{i+1/2,j}, t, u, v) = \frac{1}{\tau_\nu} \int_{-\infty}^{t} f^{eq}(x', y', t', u, v) e^{-(t-t')/\tau_\nu} dt' \tag{3.3}$$

where $x' = x_{i+1/2,j} - u(t - t')$ and $y' = y_{i+1/2,j} - v(t - t')$ is the trajectory of a particle motion. Generally, the equilibrium state f^{eq} around the center of the cell interface ($x_{i+1/2,j} = x_0,\ y_{i+1/2,j} = y_0$), and the initial time step ($t = 0$) can be approximated as

$$f^{eq}(x, y, t, u, v) = (1 + (x - x_0)a + (y - y_0)b + tA)\, g_0, \tag{3.4}$$

where g_0 is the local Maxwellian located at the center of a cell interface,

$$g_0 = \rho_0 \left(\frac{\lambda_1}{\pi}\right) e^{-\lambda_1[(u-U_0)^2+(v-V_0)^2]}. \tag{3.5}$$

Note again λ_1 is a constant. The dependence of a, b, A in Eq.(3.4) on the particle velocities can be obtained from the Taylor expansion of a Maxwellian and have the forms

$$\begin{aligned} a &= a_1 + a_2 u + a_3 v \\ &= (\frac{1}{\rho_0}\frac{\partial \rho}{\partial x} + 2\lambda_1 U_0 \frac{\partial U}{\partial x} + 2\lambda_1 V_0 \frac{\partial V}{\partial x}) - 2\lambda_1 U_0 \frac{\partial U}{\partial x} u - 2\lambda_1 V_0 \frac{\partial V}{\partial x} v, \end{aligned}$$

$$\begin{aligned} b &= b_1 + b_2 u + b_3 v \\ &= (\frac{1}{\rho_0}\frac{\partial \rho}{\partial y} + 2\lambda_1 U_0 \frac{\partial U}{\partial y} + 2\lambda_1 V_0 \frac{\partial V}{\partial y}) - 2\lambda_1 U_0 \frac{\partial U}{\partial y} u - 2\lambda_1 V_0 \frac{\partial V}{\partial y} v, \end{aligned}$$

$$\begin{aligned} A &= A_1 + A_2 u + A_3 v \\ &= (\frac{1}{\rho_0}\frac{\partial \rho}{\partial t} + 2\lambda_1 U_0 \frac{\partial U}{\partial t} + 2\lambda_1 V_0 \frac{\partial V}{\partial t}) - 2\lambda_1 U_0 \frac{\partial U}{\partial t} u - 2\lambda_1 V_0 \frac{\partial V}{\partial t} v, \end{aligned}$$

where all parameters $(\partial\rho/\partial x, \partial U/\partial x, \partial V/\partial x)$ and $(\partial\rho/\partial y, \partial U/\partial y, \partial V/\partial y)$ at $t = 0$ can be obtained from the initial reconstructions of the macroscopic variables $\partial\rho/\partial x, \partial\rho/\partial y, \partial(\rho U)/\partial x$.... For example, a 2nd-order interpolation gives

$$\rho_0 = \frac{1}{2}(\rho_{i,j} + \rho_{i+1,j})$$

$$U_0 = \frac{1}{2\rho_0}((\rho U)_{i,j} + (\rho U)_{i+1,j})$$

$$V_0 = \frac{1}{2\rho_0}((\rho V)_{i,j} + (\rho V)_{i+1,j})$$

$$\frac{\partial \rho}{\partial x} = \frac{1}{\Delta x}(\rho_{i+1,j} - \rho_{i,j})$$

$$\frac{\partial \rho}{\partial y} = \frac{1}{2\Delta y}\left(\frac{1}{2}(\rho_{i+1,j+1} + \rho_{i,j+1}) - \frac{1}{2}(\rho_{i+1,j-1} + \rho_{i,j-1})\right)$$

...

where $\Delta x, \Delta y$ are the cell sizes in the x and y directions.

After substituting Eq.(3.4) into Eq.(3.3), the final gas distribution function at a cell interface is

$$f(x_0, y_0, t, u, v) = g_0(1 - \tau_\nu(ua + vb) + (t - \tau_\nu)A). \tag{3.6}$$

The only unknown in the above equation is A, which depends on $\partial\rho/\partial t, \partial U/\partial t$ and $\partial V/\partial t$. Since

$$f^{eq}(x_0, y_0, t, u, v) = g_0(1 + At),$$

together with the compatibility condition

$$\int (f^{eq} - f) \begin{pmatrix} 1 \\ u \\ v \end{pmatrix} dudv = 0,$$

along time t and at $x = x_{i+1/2,j}$, A can be uniquely determined from

$$\int g_0(ua + vb + A) \begin{pmatrix} 1 \\ u \\ v \end{pmatrix} dudv = 0,$$

which gives

$$\begin{aligned} \frac{1}{\rho_0} \begin{pmatrix} \frac{\partial \rho}{\partial t} \\ \frac{\partial(\rho U)}{\partial t} \\ \frac{\partial(\rho V)}{\partial t} \end{pmatrix} &= -\frac{1}{\rho_0} \int (ua + vb) g_0 \begin{pmatrix} 1 \\ u \\ v \end{pmatrix} dudv \\ &= - \begin{pmatrix} a_1 < u > + a_2 < u^2 > + a_3 < uv > + b_1 < v > + b_2 < uv > + b_3 < v^2 > \\ a_1 < u^2 > + a_2 < u^3 > + a_3 < u^2 v > + b_1 < vu > + b_2 < uv^2 > + b_3 < uv^2 > \\ a_1 < uv > + a_2 < u^2 v > + a_3 < uv^2 > + b_1 < v^2 > + b_2 < uv^2 > + b_3 < v^3 > \end{pmatrix}, \end{aligned}$$

where the detail formulation of $< u^n v^m >$ can be found in the Appendix. Therefore, the above equation uniquely determines $\partial\rho/\partial t, \partial U/\partial t$ and $\partial V/\partial t$, so A is obtained.

After determining f in Eq.(3.6), the time-dependent numerical fluxes in the x-direction across the cell interface can be computed as

$$\begin{pmatrix} \mathcal{F}_\rho \\ \mathcal{F}_{\rho U} \\ \mathcal{F}_{\rho V} \end{pmatrix}_{i+1/2,j} = \int u \begin{pmatrix} 1 \\ u \\ v \end{pmatrix} g_0(1 + \tau_\nu(au + bv) + (t - \tau_\nu)A) dudv. \tag{3.7}$$

Once again, the moments of u and v can be easily obtained from the recursive relation shown in the Appendix. By integrating the above equation for a time step Δt, we get the total mass, momentum transport. Similarly, $\mathcal{G}_{i,j+1/2}$, the fluxes in the y direction can be obtained by repeating the above process in the y direction. With both fluxes in the x and y directions, we can update the flow variables inside each cell (i, j) by

$$\begin{pmatrix} \rho \\ \rho U \\ \rho V \end{pmatrix}^{n+1} = \begin{pmatrix} \rho \\ \rho U \\ \rho V \end{pmatrix}^{n} + \int_0^{\Delta t} (\frac{1}{\Delta x}(\mathcal{F}_{i-1/2,j} - \mathcal{F}_{i+1/2,j}) + \frac{1}{\Delta y}(\mathcal{G}_{i,j-1/2} - \mathcal{G}_{i,j+1/2}))dt - \begin{pmatrix} 0 \\ 0 \\ \rho^n \beta G_0 (T^n - T_m) \end{pmatrix} \Delta t,$$

where the effect from Eq.(3.2) has been accounted for in the above equation.

Once Eq.(2.2) is solved, the scheme for Eq.(2.3) can be constructed similarly. For example, we can expand h^{eq} as

$$h^{eq}(x, y, t, u, v) = h_0(1 + (x - x_0)a_h + (y - y_0)b_h + tA_h),$$

where

$$h_0 = (\rho_0 T_0) \left(\frac{\lambda_2}{\pi}\right) e^{-\lambda_2((u-U_0)^2 + (v-V_0)^2)}$$

at a cell interface, and

$$\begin{aligned} a_h &= a_{h1} + a_{h2}u + a_{h3}v \\ &= (\frac{1}{\rho_0 T_0} \frac{\partial(\rho T)}{\partial x} + 2\lambda_2 U_0 \frac{\partial U}{\partial x} + 2\lambda_2 V_0 \frac{\partial V}{\partial x}) - 2\lambda_2 U_0 \frac{\partial U}{\partial x} u - 2\lambda_2 V_0 \frac{\partial V}{\partial x} v, \end{aligned}$$

$$
\begin{aligned}
b_h &= b_{h1} + b_{h2}u + b_{h3}v \\
&= (\frac{1}{\rho_0 T_0}\frac{\partial(\rho T)}{\partial y} + 2\lambda_2 U_0\frac{\partial U}{\partial y} + 2\lambda_2 V_0\frac{\partial V}{\partial y}) - 2\lambda_2 U_0\frac{\partial U}{\partial y}u - 2\lambda_2 V_0\frac{\partial V}{\partial y}v,
\end{aligned}
$$

$$
\begin{aligned}
A_h &= A_{h1} + A_{h2}u + A_{h3}v \\
&= (\frac{1}{\rho_0 T_0}\frac{\partial(\rho T)}{\partial t} + 2\lambda_2 U_0\frac{\partial U}{\partial t} + 2\lambda_2 V_0\frac{\partial V}{\partial t}) - 2\lambda_2 U_0\frac{\partial U}{\partial t}u - 2\lambda_2 V_0\frac{\partial V}{\partial t}v,
\end{aligned}
$$

which are closely related to the coefficients of a, b and A. In other words, the evolution of h is not totally independent of the evolution f, and $\partial U/\partial x, \partial V/\partial x, ...$ in the above equations are the same as the corresponding terms in the equations defining a, b, A earlier. Hence, the only unknowns are $T_0, \partial T/\partial x, \partial T/\partial y$ and $\partial T/\partial t$. In order to determine all unknowns, at $t = 0$, the following interpolations can be used to get $\rho_0 T_0$ and $\partial(\rho T)/\partial x, \partial(\rho T)/\partial y$. The linear reconstruction of thermal energy ρT is necessary with

$$
\rho_0 T_0 = 0.5((\rho T)_{i,j} + (\rho T)_{i+1,j}),
$$

and

$$
\frac{\partial(\rho T)}{\partial x} = \frac{1}{\Delta x}((\rho T)_{i+1,j} - (\rho T)_{i,j}),
$$

$$
\frac{\partial(\rho T)}{\partial y} = \frac{1}{2\Delta y}((\rho_0 T_0)_{i+1/2,j+1} - (\rho_0 T_0)_{i+1/2,j-1}).
$$

The final solution of h at the center of the cell interface is

$$
h(x_0, y_0, t, u, v) = h_0(1 - \tau_c(ua_h + vb_h) + (t - \tau_c)A_h), \tag{3.8}
$$

and the $\partial T/\partial t$ term in A_h is determined by applying the compatibility condition

$$
\int (h^{eq} - h)dudv = 0,
$$

along (x_0, y_0, t), which similarly gives

$$
\int A_h h_0 dudv = -\int (a_h u + b_h v)h_0 dudv.
$$

Once h is determined in Eq.(3.8), the numerical flux for the thermal energy is

$$
\mathcal{F}_{\rho T} = \int uhdudv,
$$

and the thermal energy inside each cell can be subsequently updated.

4. Results. The Rayleigh-Bénard problem offers a first approach to a complicated convective flow. In this case, with the gravitational force in the vertical direction a horizontal layer of viscous fluid is heated from the bottom while the top boundary is maintained at a lower temperature. When the temperature difference between the top and bottom boundaries is increased above a certain threshold, the static conduction state becomes unstable to any small disturbance and the system become convective.

In our calculations, the horizontal and vertical length scales are $L = 2.0$ and $H = 1.0$, respectively. The temperatures at the bottom and top are $T_{bottom} = 1.0, T_{top} = 0.0$, with the difference $\Delta T = 1.0$. Non-slip boundary conditions are implemented at the bottom and top boundaries by reversing the flow velocities in

the 'ghost' cell next to the simulation domain. Periodic boundary conditions are used for the temperature along the sides of the box. In our current study, we fix $G_0 = 1.0$ and $\beta = 0.1$.

The Rayleigh number is defined as

$$R = \frac{\beta \Delta T G_0 H^3}{\nu k}.$$

From the above relation and $Pr = \nu/k$, the viscosity coefficient can be determined:

$$\nu = \sqrt{\frac{\beta \Delta T G_0 H^3 Pr}{R}}.$$

Consequently, the collision time τ_ν in Eq.(2.2) is fixed with

$$\tau_\nu = 2\lambda_1 \nu,$$

and τ_c in Eq.(2.3) is

$$\tau_c = \tau_\nu \frac{\lambda_2}{\lambda_1 Pr}.$$

Since in the simulations, the CFL time step Δt is almost a constant, in order to keep the collision time τ_ν to be around $10^{-1}\Delta t$, we have to choose λ_1 properly. In most calculations, λ_1 is on the order of 10^{-1}. Although the numerical scheme is general for any Pr, we used $P_r = 1,\ \lambda_1 = \lambda_2$ and $\tau_\nu = \tau_c$.

As a first test, we tried to get the critical Rayleigh number for the onset of thermal convection. With a 80×40 mesh, we have simulated this problem with two supercritical Rayleigh numbers $R = 1720$ and $R = 1735$ separately. In each case, we calculate the maximum y-component velocity in the whole computational domain at each time step. The time-dependent amplitude of the y-velocity on a 80×40 mesh is shown in Figure 5.1, from which we can estimate the critical Rayleigh number by fitting the curve to $V \sim \exp(\alpha(R - R_c)t)$, where R_c is the critical Rayleigh number. From the exponential growth rates, we found that the critical Rayleigh number in our calculations is $R_c = 1711.17$, which is 0.22% away from the theoretical value 1707.76 (which is actually for a box of width 2.0158). For other meshes, the calculated critical Rayleigh numbers are listed in Table 1.

Table 1. Critical Rayleigh numbers calculated on different meshes. The error is calculated relative to the theoretical value.

Grid Size	Ra_c	Error
20×10	1756.22	2.84%
40×20	1729.43	1.27%
80×40	1711.45	0.22%
theory	1707.76	

Once the Rayleigh-Bénard convection is stabilized, the heat transfer between the top and bottom is greatly enhanced. The enhancement of the heat transfer can be described by the Nusselt number,

$$N_u = 1 + \frac{< VT >}{k\Delta T/H},$$

where V is the vertical velocity, ΔT is the temperature difference between the bottom and top walls, H is the height of the box, and $< ... >$ represents the average over the whole flow domain. Figure 5.2 is the calculated relationship between the Nusselt number and the Rayleigh number. The simulation results by

Clever and Busse [4] is also included. As shown in the figure, our results are very close to those by Clever and Busse. But, at higher Rayleigh numbers, our values of the Nusselt number is a little bit smaller than that in [4], and thus underestimating the amount of heat transfer. Similar results are obtained using lattice Boltzmann methods[12, 8].

Typical temperature and stream function contours are shown in Figures 3 - 8 with $Ra = 5,000$, $10,000$ and $50,000$. As the Rayleigh number increases, two trends were observed for the temperature distribution: enhanced mixing of the hot and cold fluids and an increase in the temperature gradients near the bottom and top boundaries. Both trends enhance the heat transfer in the box.

As another benchmark problem, we have tried one case in [5]. This problem is that of the two-dimensional Boussinesq flow in a square with $H = L = 1.0$ and Prandtl number $Pr = 0.71$, which is done by setting $\lambda_1 = \lambda_2$ and $\tau_c = \tau_\nu / Pr$ in our code. Both velocity components are zero on the boundaries. The horizontal walls are insulated, and the vertical sides are at temperatures $T_{left} = 1.0$ and $T_{right} = 0.0$. In this case, the Nusselt number is defined as

$$N_u = 1 + \frac{< UT >}{k\Delta T / L}.$$

The results for the streamline and temperature contours at $R = 10^5$ are shown in Figure 5.9 and 5.10. With $R = 10^5$, the average Nusselt number in the whole domain is listed in Table 2 for different mesh sizes. Contrary to the last test case, our result overestimates the heat transfer. A larger Nusselt number is obtained.

Table 2. Nusselt numbers calculated on different meshes. The error is calculated relative to the numerical result in [5].

Grid Size	Nusselt Number	Error
20×20	4.590	1.77%
40×40	4.563	1.17%
80×80	4.540	0.66%
reference [5]	4.510	

5. Conclusion. In this paper, a two-temperature gas-kinetic BGK model for convective thermal flow is constructed. A numerical scheme has subsequently been developed. As an application, the 2D Rayleigh-Bénard case is studied. The simulation results are very close to those obtained by other methods. To study the incompressible flow phenomena using the compressible model is an attractive research area. In order to simulate thermal effects in an incompressible fluid, the decoupling of the energy equation from the mass and momentum equations seems necessary, because the relation between temperature and volume changes are different for incompressible and compressible fluids. Compared with the lattice BGK methods, the current approach with continuous particle velocity has advantages in terms of stability and efficiency. The time step used in the current method is the CFL time step which is about one order of magnitude larger than the particle collision time which is usually used in the lattice BGK method[11].

In this paper, the temperature evolution equation only includes advection and diffusion terms. The viscous heating term in the Navier-Stokes energy equation is ignored due to the simplicity of the model. The construction of a two-temperature BGK model with the viscous heating term in the thermal energy evolution equation is an interesting and important problem. The research in this direction will help us to find an efficient kinetic scheme to simulate incompressible flow, and pave the way to simulate a flow mixing compressible gas and incompressible liquid.

Acknowledgments. We would like to thank Dr. X. He for his helpful discussion and advice in this work, and thank Dr. L. Luo for his valuable comments.

Appendix: Moments of the Maxwellian Distribution Function. In the gas-kinetic scheme, we need to evaluate moments of the Maxwellian distribution function with unbounded integration limits. Here, we list some general formulas.

Firstly, we assume that the Maxwellian distribution for a two-dimensional flow is

$$g = \rho(\frac{\lambda}{\pi})e^{-\lambda((u-U)^2+(v-V)^2)}.$$

Then, by introducing the following notation for the moments of g,

$$\rho < ... >= \int (...)gdudv,$$

the general moment formula becomes

$$< u^n v^m >=< u^n >< v^m >,$$

where n, m are integers. When the integration limits are from $-\infty$ to $+\infty$, we have

$$< u^0 >= 1$$

$$< u >= U$$

..

$$< u^{n+2} >= U < u^{n+1} > + \frac{n+1}{2\lambda} < u^n > .$$

Similarly,

$$< v^0 >= 1$$

$$< v >= V$$

..

$$< v^{m+2} >= V < v^{m+1} > + \frac{m+1}{2\lambda} < v^m > .$$

REFERENCES

[1] P.L. Bhatnagar, E.P. Gross, and M. Krook, *A Model for Collision Processes in Gases I: Small Amplitude Processes in Charged and Neutral One-Component Systems*, Phys. Rev., **94** (1954), pp. 511-525.

[2] S. Chandrasekhar, *Hydrodynamic and Hydromagnetic Stability*, Oxford University Press (1961).

[3] S. Chen and G.D. Doolen, *Lattice Boltzmann Method for Fluid Flows*, Ann. Rev. Fluid Mech., **30** (1998), pp. 329.

[4] R.M. Clever and F.H. Busse, *Transition to Time-dependent Convection*, J. Fluid Mech., **65** (1974), pp. 625.

[5] G. De Vahl Davis, *Natural Convection of Air in a Square Cavity: a Bench Mark Numerical Solution*, Int. J. for Numer. Methods in Fluids, **3** (1983), pp. 249-264.

[6] P. G. Drazin and W. H. Reid, *Hydrodynamic Stability*, Cambridge University Press (1981).

[7] X. He, X. Shan, and G. Doolen, *Discrete Boltzmann Equation Model for Nonideal Gases*, Phys. Rev. E,**57** (1998), pp. 13.

[8] X.Y. He, S. Chen, and G. Doolen, *A Novel Thermal Model for the Lattice Boltzmann Method in Incompressible Limit*, J. Comput. Phys. (1998), in press.

[9] X. He and L. Luo, *Lattice Boltzmann Method for the Incompressible Navier-Stokes Equation*, J. Stat. Phys., **88** (1997), pp. 927.

[10] M.J. Ivings, D.M. Causon, and E.F. Toro, *On Riemann Solvers for Compressible Liquids*, Int. J. Numer. Methods in Fluids, **28** (1998), pp. 395.

[11] P. Pavlo, G. Vahala, L. Vahala, and M. Soe, *Linear-stability Analysis of Thermal-lattice Boltzmann Models*, J. Comput. Phys., **139** (1998), pp. 79.

[12] X. Shan, *Solution of Rayleigh-Bénard Convection Using a Lattice Boltzmann Method*, Phys. Rev. E, **55** (1997), pp. 2780.

[13] M.D. Su, K. Xu, and M.S. Ghidaoui, *Low Speed Flow Simulation by the Gas-Kinetic Scheme*, accepted by J. Comput. Phys. (1998).

[14] K. Xu, *Gas-Kinetic Schemes for Unsteady Compressible Flow Simulations*, 29th CFD Lecture Series, von Karman Institute for Fluid Dynamics (1998).

[15] K. Xu, *Numerical Hydrodynamics from Gas-Kinetic Theory*, Ph.D. Thesis, Columbia University (1993).

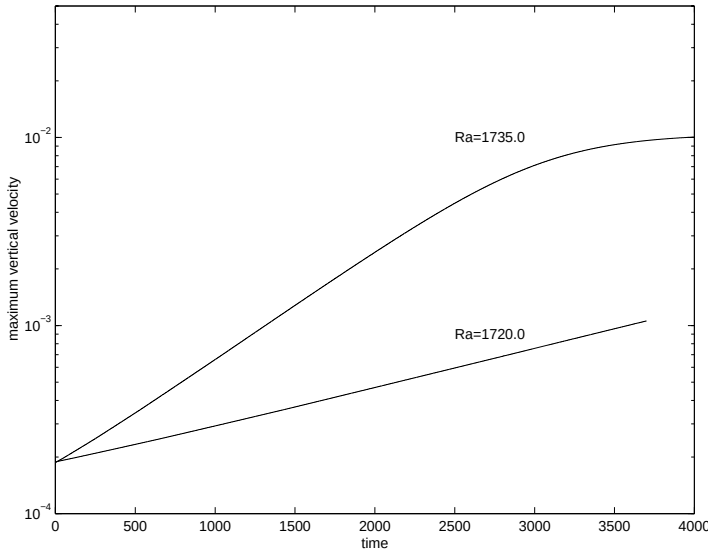

FIG. 5.1. *Time history of the maximum vertical velocities.*

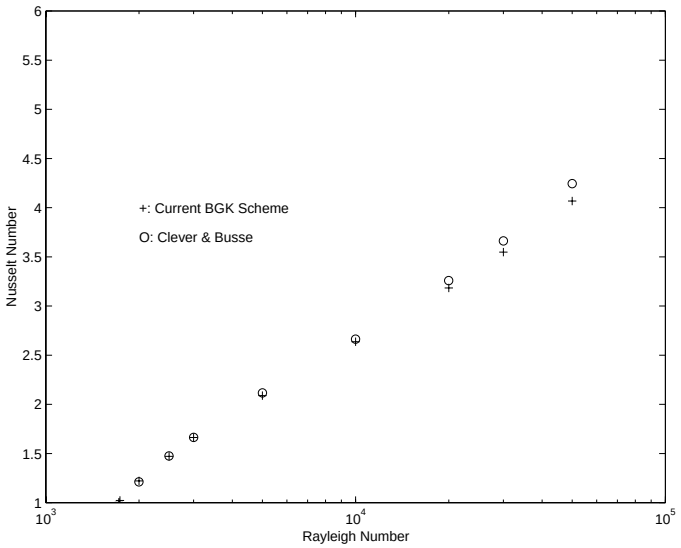

FIG. 5.2. *The dependence of Nusselt number on Rayleigh number. The simulation results by Clever and Busse [4] are also included.*

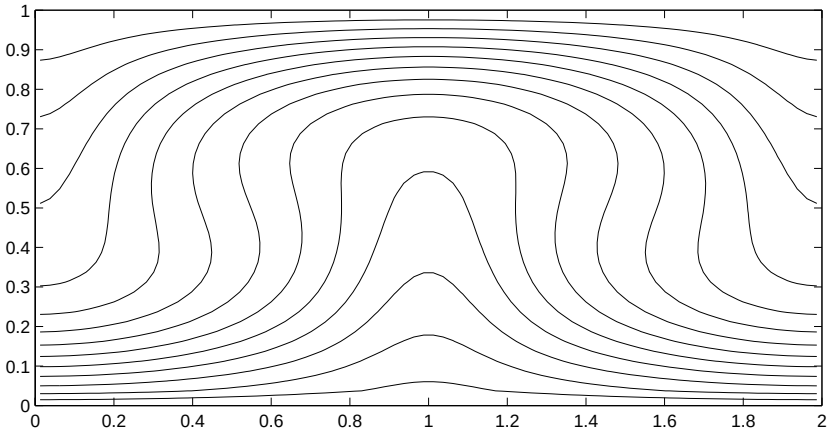

FIG. 5.3. *Temperature contours at* $R = 5000$

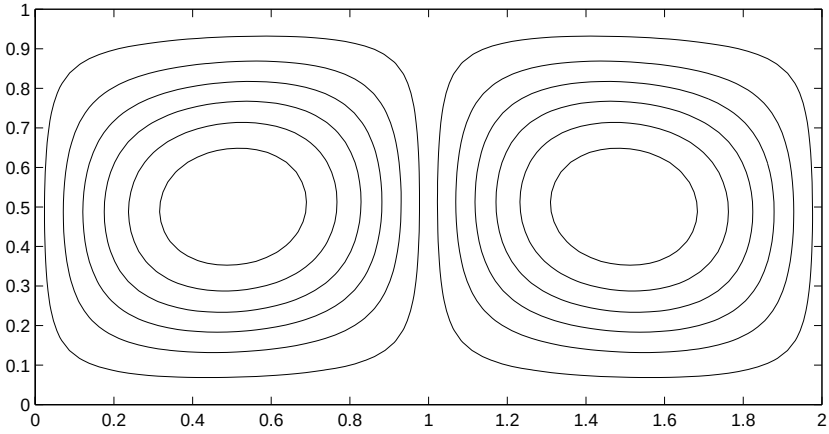

FIG. 5.4. *Stream function contours at* $R = 5000$

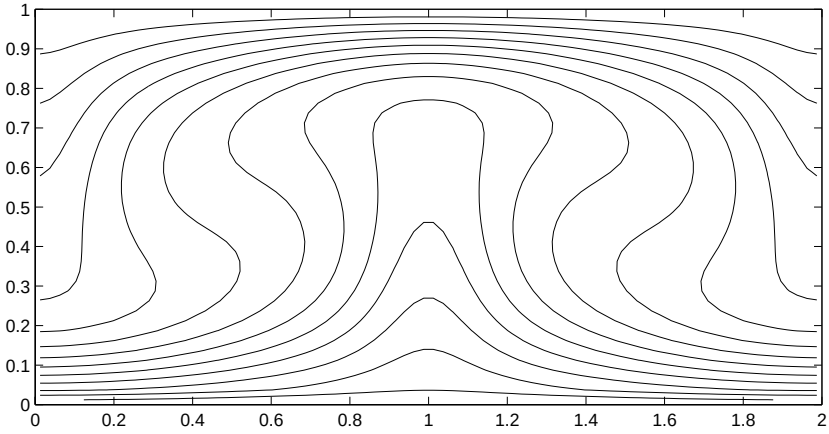

FIG. 5.5. *Temperature contours at* $R = 10000$

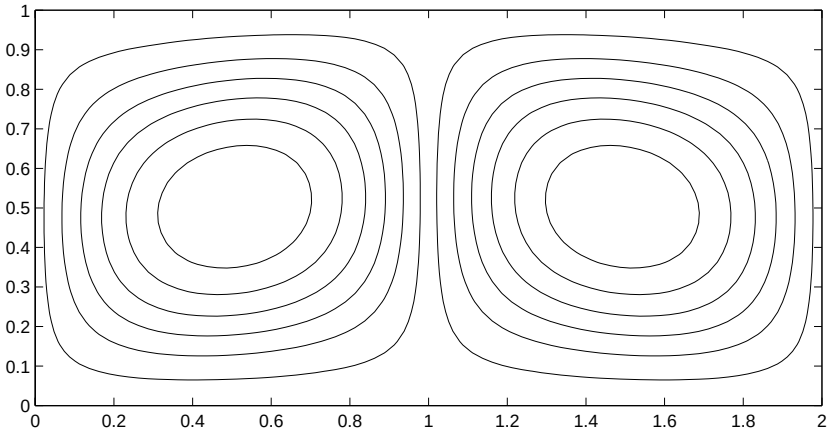

FIG. 5.6. *Stream function contours at* $R = 10000$

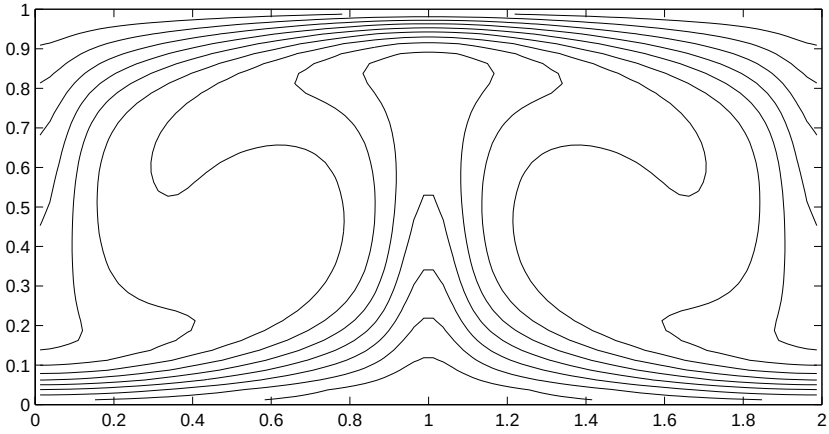

FIG. 5.7. *Temperature contours at* $R = 50000$

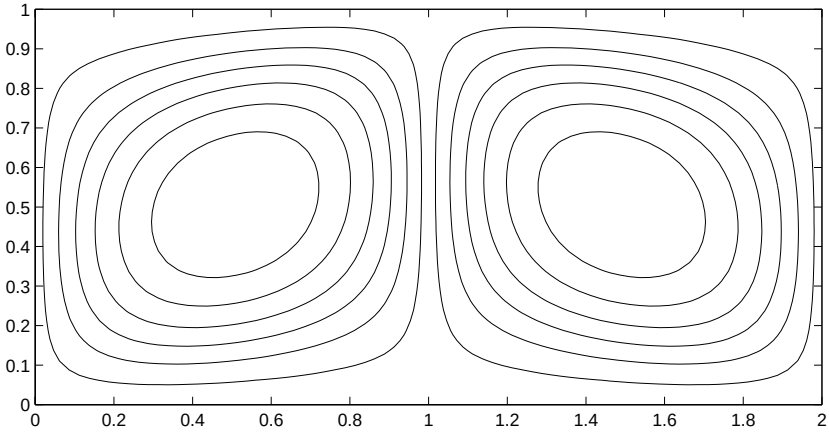

FIG. 5.8. *Stream function contours at* $R = 50000$

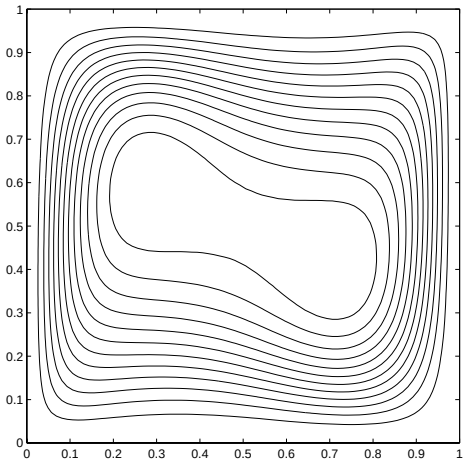

FIG. 5.9. *Stream function contours at* $R = 100000$

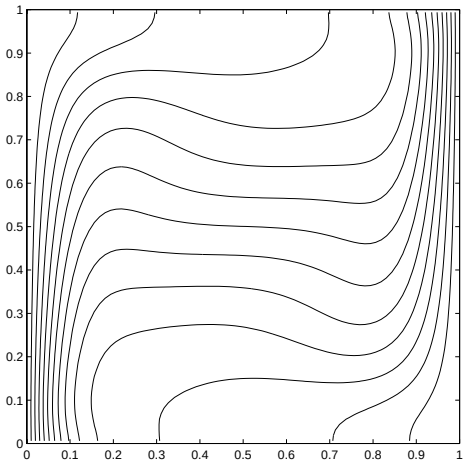

FIG. 5.10. *Temperature contours at* $R = 100000$